PROCEEDINGS OF SCIENCE

Cosmic antimatter signatures from primordial back holes

Valentina De Romeri,[a] **Fiorenza Donato,**[b,c] **David Maurin,**[d] **Lorenzo Stefanuto**[b,*] **and Agense Tolino**[a]

[a] *Instituto de Física Corpuscular (CSIC-Universitat de València), Parc Científic UV C/ Catedrático José Beltrán, 2 46980 Paterna (Valencia) - Spain*

[b] *Dipartimento di Fisica, Università di Torino, and INFN, Sezione di Torino Via P. Giuria 1, Torino, Italy*

[c] *Theoretical Physics Department, CERN, Esplanade des Particules 1, CH-1211 Geneva 23, Switzerland*

[d] *LPSC, Université Grenoble-Alpes, CNRS/IN2P3, 38026, Grenoble, France*

E-mail: deromeri@ific.uv.es, fiorenza.donato@unito.it, dmaurin@lpsc.in2p3.fr, lorenzo.stefanuto@unito.it, atolino@ific.uv.es

Primordial black holes (PBHs) are hypothetical objects that may have formed in the early Universe and could account for part of the dark matter content. Through Hawking radiation (HR), PBHs can emit particles that may ultimately lead to the production of antinuclei such as antiprotons and antideuterons, which subsequently propagate through the Galaxy and reach Earth as cosmic rays (CRs). These particles are expected to exhibit fluxes peaking at GeV energies, making them promising messengers for new physics. In this work, we re-examine the production of CR antiprotons and antideuterons from PBH evaporation. Our analysis employs lognormal PBH mass distributions, up-to-date CR propagation models, and an improved coalescence approach for modeling antideuteron formation. We compare our predictions to the latest AMS-02 measurements of the antiproton flux. We find that the AMS-02 antiproton data impose stringent constraints on the local PBH density, with limits that strongly depend on the parameters characterizing the lognormal mass distributions. These bounds are comparable to, or slightly stronger than, existing constraints derived from other astrophysical messengers. We further explore the prospects for detecting antideuterons in future experiments. Any potential observation of antideuterons by AMS-02 or GAPS would likely indicate new physics beyond standard secondary production processes. However, given the constraints on the local PBH density imposed by the AMS-02 antiproton data, such a signal could only partly be explained by PBH evaporation.

The results presented here are taken from our recent study, published in *Physical Review D* [Phys. Rev. D 112 (2025) 2, 023003]. For further details, we refer the reader to that work.

39th International Cosmic Ray Conference (ICRC2025)
15–24 July 2025
Geneva, Switzerland

*Speaker

PoS(ICRC2025)530

1. Introduction

PBHs are a proposed class of black holes that may have formed in the early Universe through various mechanisms, such as the collapse of primordial density fluctuations before Big Bang nucleosynthesis [1]. In recent years, PBHs have attracted renewed attention, partly due to gravitational-wave detections by LIGO-Virgo-KAGRA [2], which, while confirming the existence of astrophysical black holes, have also provided new opportunities to examine whether some of these events might originate from PBHs.

PBHs have long been proposed as potential dark matter (DM) candidates, although only those within the asteroid-mass range (10^{17} g to 10^{22} g) could account for the entirety of DM. [3] According to Hawking radiation [4], PBHs may produce particles across a broad spectrum, including photons, neutrinos, and antimatter such as positrons, antiprotons, and even heavier antinuclei. These signatures provide promising probes for the existence of light PBHs.

In particular, CR antiprotons and antideuterons offer complementary messengers to photons and neutrinos. Antinuclei from PBH evaporation are expected to peak at lower energies than secondary antinuclei produced by CR scattering with the interstellar medium, making low-energy data especially sensitive to PBH contributions. While CR antiprotons have been precisely measured by AMS-02 [5], antideuterons remain unobserved so far, with only future prospects from AMS-02 and the forthcoming GAPS experiment [6] .

In this work, we revisit the signatures of antiprotons and antideuterons from PBH evaporation, derive new constraints on the local PBH density using AMS-02 antiproton data [5] and discuss implications for the fraction of DM composed of PBHs and for future antideuteron searches.

2. Evaporation of PBHs into antimatter

PBHs are expected to span a broad mass range, which can significantly influence their astrophysical signatures. We can define the following quantity to account for the PBH number density per interval of initial mass $M_{\rm in}$,

$$g(r, z, M_{\rm in}) \equiv M_{\rm in} \frac{{\rm d}n_{\rm PBH}}{{\rm d}M_{\rm in}} = M_{\rm in} \frac{{\rm d}^2 N_{\rm PBH}}{{\rm d}M_{\rm in}{\rm d}V}\,, \tag{1}$$

where $n_{\rm PBH}$ is the PBH number density, ${\rm d}V$ is the volume interval and $N_{\rm PBH}$ refers to the overall number of PBHs. Different formation scenarios motivate different functional forms for this distribution. A commonly used parametrization is the lognormal distribution [7], characterized by a peak mass μ_c and a width σ. This choice is motivated by scenarios where PBHs form from a symmetric peak in the primordial power spectrum, and is given by

$$g(r, z, M_{\rm in})|_{\rm ln} = \rho_{\rm PBH}(r, z) \frac{\mathcal{A}}{\sqrt{2\pi}\sigma M_{\rm in}} \exp\left[-\frac{\log^2(M_{\rm in}/\mu_c)}{2\sigma^2}\right], \tag{2}$$

where $\rho_{\rm PBH}(r, z)$ denotes the PBH mass density at the cylindrical galactic coordinates r and z. In the following, we define $\rho_{\rm PBH} \equiv \rho_{\rm PBH}(R_\odot, 0)$ as the local PBH density at the position of the Sun, which acts as an overall normalization of the mass distribution.

Alternative scenarios consider power-law spectra, arising for instance from scale-invariant primordial perturbations or cosmic string collapse, or a monochromatic mass function where all

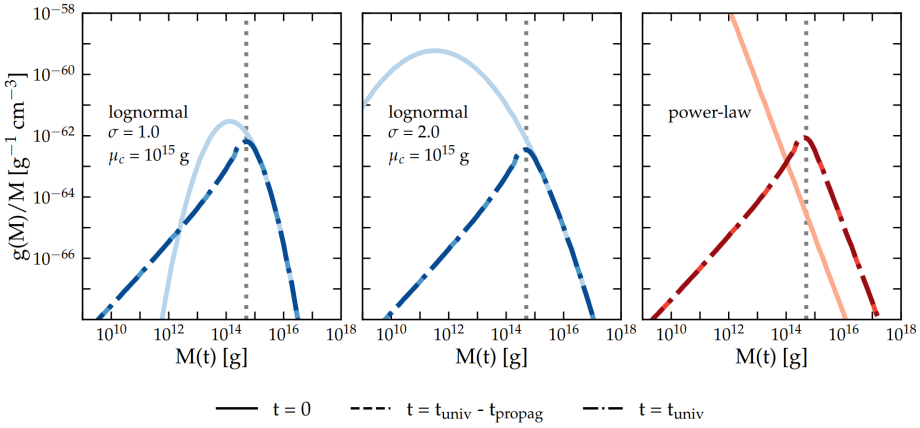

Figure 1: PBH mass distributions $g(M)/M$ evolved over time. The lognormal case from Eq. (2) is shown in blue for $\mu_c = 10^{15}$ g and various σ, while the last panel shows a power-law evolution. Solid lines refer to the distribution at the time of formation; the dot-dashed (dashed) lines show the same distribution evolved until the age of the Universe (accounting for the average propagation time of CR antiprotons). The vertical dotted gray line marks the initial mass $M^*_{\rm in} = 5 \times 10^{14}$ g for a PBH that is evaporating completely today.

PBHs share a single mass $M_{\rm mc}$. In our analysis, we adopt lognormal mass functions with various σ values. Extended distributions are known to alter phenomenological constraints compared to simpler monochromatic assumptions. This has important implications for evaluating PBH contributions to CR signals and their potential role as dark matter candidates.

According to Hawking's prediction [4], black holes radiate quasi-thermally, with a temperature inversely proportional to their mass. The evaporation rate increases as the mass decreases, since hotter black holes emit more energetic particles and more degrees of freedom become kinematically accessible. As a result, PBH extended mass distributions evolve significantly over cosmic time. This evolution can be computed by solving the mass-loss equation numerically and leads to a present-day PBH distribution which differs notably from the initial one.

We illustrate this behavior in Fig. 1, which shows the evolved mass distributions for various initial PBH spectra. All extended mass functions develop a low-mass tail below $M \sim 10^{14}$ g, with their slopes converging to a shape proportional to M^2 across different models. This low-mass region is especially relevant for the production of antiprotons and antideuterons, since these particles are efficiently produced only by PBHs with masses $M \lesssim 10^{14}$ g. Consequently, the universal M^2-like behavior of the evolved distributions in this mass range will translate into similar spectral shapes for the resulting antinuclei fluxes, as we will discuss in the following.

Turning to antimatter production, PBHs do not directly emit antinuclei. Instead, quarks, gluons, and bosons emitted via HR can hadronize into composite states, including antiprotons and antideuterons. The source term of antinuclei from PBHs is computed as

$$Q_{\bar{p}(\bar{d})}(r,z,E) = \int_{M_{\rm min}}^{M_{\rm max}} {\rm d}M \, \frac{g(r,z,M)}{M} \sum_i \int_{m_i}^{\infty} {\rm d}E_i \, \left.\frac{{\rm d}^2 N_i}{{\rm d}E_i {\rm d}t}\right|_{\rm HR} \frac{{\rm d}N_{i\to\bar{p}(\bar{d})}}{{\rm d}E}(E,E_i)\,, \qquad (3)$$

where i runs over all directly emitted species. The fragmentation functions ${\rm d}N_{i\to\bar{p}(\bar{d})}/{\rm d}E$ are extracted from `CosmiXs` [8, 9] and account for hadronization. For antideuterons, the coalescence model relies on the state-of-the-art Argonne-Wigner approach [9]. We implement the HR spectra

$\mathrm{d}^2N_i/\mathrm{d}E_i\mathrm{d}t|_{\mathrm{HR}}$ from `BlackHawk v2.3` [10]. The convolution with fragmentation functions is performed with a custom `Python` code.

The computed sources exhibit universal energy-spectrum shapes, one for each antinucleus species. Despite varying initial mass distribution parameters (e.g. μ_c and σ), the spectra differ essentially by an overall normalization, while the spectral shape remains practically identical. This arises because of the universal M^2-like behavior of the evolved distributions discussed above.

3. Propagation in the galaxy

Once the production source spectra of antinuclei from PBH evaporation are computed, they must be propagated through the Galaxy to enable comparison with CR data. We follow the CR transport formalism used in [11], adopting a two-zone cylindrical geometry with radius $R_G = 20$ kpc and variable half-height L of the diffusion volume. We assume a NFW spatial distribution of PBHs [11]. Propagation is governed by the diffusion equation, including spatial diffusion, convection, energy losses, and reacceleration. We solve this equation semi-analytically with the `USINE` code [12].

The diffusion coefficient $K(R)$ exhibits possible rigidity breaks and depends on several transport parameters constrained by CR secondary-to-primary ratios. We consider benchmark propagation models (BIG, SLIM, QUAINT) following [11, 13], and adopt BIG as our fiducial choice.

Secondary and tertiary antinuclei production from standard CR interactions in the interstellar medium are included, following [13]. Solar modulation is accounted for via the force-field approximation, considering an average solar modulation potential $\langle\phi_{FF}\rangle = 731$ MV [13, 14].

An important feature is that the propagated fluxes of PBH-induced primary antinuclei at Earth share universal spectral shapes, differing only by a normalization factor. This property is inherited from the universality of the spectral shapes of the sources described above.

4. Statistical analysis

We consider the most recent data on CR antiprotons collected by AMS-02 in the rigidity range 1-525 GV [5]. These measurements allow setting stringent constraints on antiprotons possibly produced by PBH evaporation. Following [11], we adopt a log-likelihood function combining the χ^2 between model predictions and data, and a penalty term on L:

$$-2\ln\mathcal{L}(L,\mu) = \sum_{i,j} x_i\,(C^{-1})_{ij}\,x_j + \left\{\frac{\log L - \log\hat{L}}{\sigma_{\log L}}\right\}^2, \tag{4}$$

where $x_i = \phi_i^{\mathrm{exp}} - \phi_i^{\mathrm{th}}(L,\mu)$, with ϕ_i denoting the flux value in the i-th energy bin, and μ collectively representing the PBH parameters, namely ρ_{PBH}, μ_c, and σ. The covariance matrix C accounts for experimental uncertainties (statistical and systematic) and for theoretical uncertainties in secondary production and transport [13]. The best-fit halo size $\hat{L}$ and its uncertainty $\sigma_{\log L}$ are taken from [15].

A fully consistent analysis would involve scanning over all transport and PBH parameters simultaneously. Instead, following [11], we adopt a faster approach where propagation uncertainties enter via C and the penalty on L. The primary PBH flux is pre-computed on a grid of L and μ_c

values using USINE, and scaled for arbitrary $\rho_{\rm PBH}$. Secondary fluxes and the covariance matrix are reused from previous works [11, 13].

To derive upper limits (UL) on $\rho_{\rm PBH}$, for fixed values of μ_c and σ, we rely on the following likelihood ratio (LR):

$$\mathrm{LR}(\rho_{\rm PBH}) = -2\ln\mathcal{L}(L_{\rm min}, \rho_{\rm PBH}) + 2\ln\mathcal{L}(L', \rho'_{\rm PBH})\,, \tag{5}$$

where the numerator is evaluated at the halo size maximizing the likelihood for a given $\rho_{\rm PBH}$, and the denominator at the global best fit. Assuming Wilks' theorem, LR follows a χ^2 distribution with one degree of freedom. We set 95% confidence level (CL) UL by requiring LR = 3.84 [11].

5. Results for the $\rho_{\rm PBH}$ upper bounds

Figure 2 (left) shows the top-of-atmosphere (TOA) antiproton flux from secondary production and PBH evaporation, assuming $\mu_c = 10^{14}$ g and $\sigma = 1$. For PBH-induced fluxes, we display both the flux UL (solid blue), computed considering the 95% CL UL on $\rho_{\rm PBH}$ (for this choice of μ_c and σ, $\rho^{\rm UL}_{\rm PBH} = 1.9\times10^{-10}$ GeV cm^{-3}), and, for illustration, the corresponding best-fit flux (dotted blue). These are shown together with the secondary flux (solid red) and the total flux (black). The data are well reproduced by the secondary background alone, implying that any PBH contribution must remain subdominant to avoid overshooting the low-energy measurements. The PBH-induced flux peaks around 1–2 GeV, slightly shifted to lower energies compared to the secondary component. This peak arises from a complex interplay of Hawking radiation, mass distribution convolution, hadronization, Galactic propagation, and solar modulation effects. Since the spectral shape is stable under variations of μ_c and σ, these changes translate into a simple rescaling of $\rho_{\rm PBH}$. As a result, the flux UL remains unaffected. Our likelihood analysis inherently includes all relevant uncertainties (propagation, cross-sections, solar modulation), resulting in a single robust UL curve without additional error bands.

We further assess the impact of the GAPS experiment, which is expected to provide low-energy antiproton measurements in the 0.07-0.21 GeV range. The right panel of Fig. 2 shows the PBH-induced flux UL (blue) obtained from a combined analysis of AMS-02 data and simulated GAPS data corresponding to three 35-day flights [16], assuming identical solar modulation conditions. Including GAPS data could improve the constraints on $\rho_{\rm PBH}$ by a factor of ~ 2.

From the ULs on $\rho_{\rm PBH}$, we can easily derive constraints on the fraction of DM composed by PBHs, defined as $f_{\rm PBH} = \rho_{\rm PBH}/\rho_\odot$, considering the DM local density $\rho_\odot = 0.385\,\mathrm{GeV\,cm^{-3}}$. Figure 3 shows the 95% CL constraints on $f_{\rm PBH}$, for different values of μ_c and σ. The tightest bound, $f_{\rm PBH} \lesssim 10^{-11}$, is found at $\mu_c = M^*$ for $\sigma = 0.1$. Broader mass distributions extend sensitivity to higher masses, also covering part of the so-called asteroid-mass region.

We also compare our result for $\sigma = 1$ with existing limits from other cosmic messengers [17] (Fig. 3, right panel). Although the methodologies and assumptions differ, our analysis with AMS-02 antiproton data provides highly competitive constraints.

6. Perspectives with antideuteron measurement

Figure 4 shows the TOA PBH-induced antideuteron flux, normalized to the 95% CL UL on $\rho_{\rm PBH}$ from our antiproton analysis. Although the PBH flux UL (solid blue) overtakes the secondary

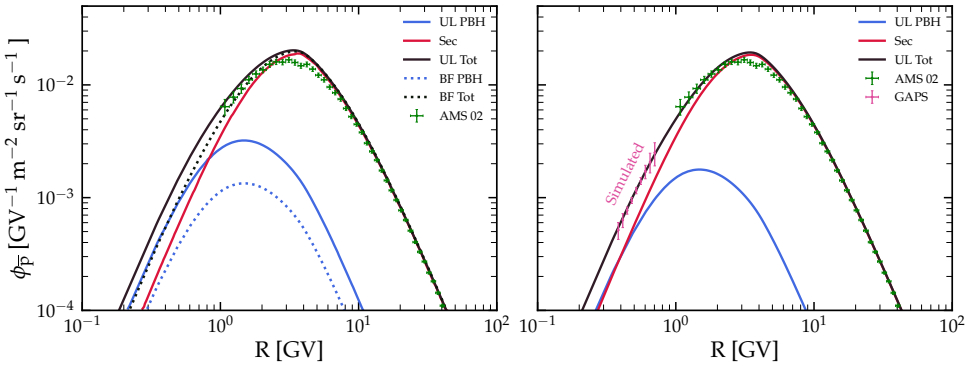

Figure 2: Fluxes of TOA antiprotons: secondary flux (solid red line), primary flux from PBH evaporation (blue lines), and total flux (black lines). Left panel: the blue solid curve is the 95% CL UL on the PBH-induced flux; for illustration purpose, the dashed lines show the PBH (and total) fluxes fitting best the data. Green symbols stand for AMS-02 data [5]. Right panel: 95% CL UL fluxes computed considering the combination of AMS-02 data and GAPS simulated data [16] (pink symbols).

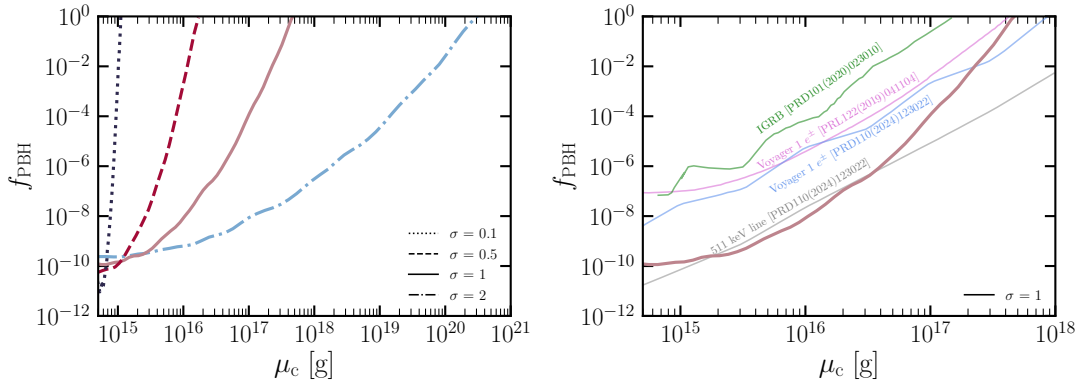

Figure 3: Antiproton bounds on the PBH fraction of the local DM density, $f_{\rm PBH} = \rho_{\rm PBH}/\rho_\odot$, as a function of μ_c. Left panel: 95% CL exclusion limits based on AMS-02 data [5] for a lognormal PBH mass distribution with width $\sigma = 0.1$ (dotted), 0.5 (dashed), 1 (solid) and 2 (dot-dashed). Right panel: our result (red thick line) for $\sigma = 1$, compared with other bounds from different messengers [17].

component (solid red) below 3 GeV, it remains below the projected sensitivities of GAPS and AMS-02 (shaded bands) [18, 19]. Different solar modulation conditions (dashed and dot-dashed curves) does not change this conclusion. Moreover, as in the case of antiprotons, variations in μ_c and σ do not provide differences in the UL fluxes, since they only rescale the normalization (via $\rho_{\rm PBH}$) and do not affect the universal shape of the spectra. Propagation uncertainties are fully included in our likelihood framework, and residual coalescence uncertainties are at the few-percent level [9].

7. Conclusions

We have revisited the CR antiproton and antideuteron signatures of PBH evaporation, extending previous studies by adopting a lognormal PBH mass distribution, up-to-date Galactic propagation

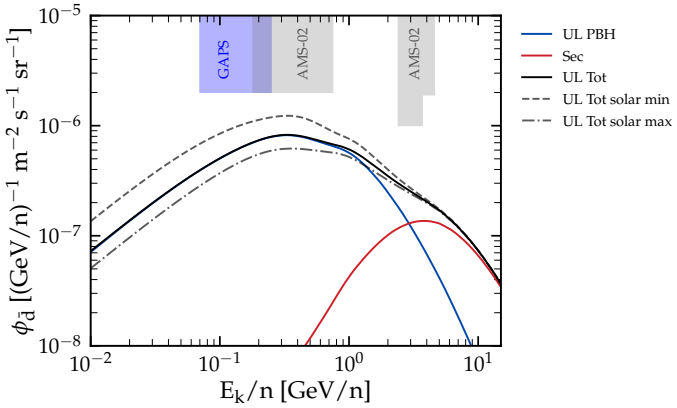

Figure 4: Fluxes of TOA antideuterons from secondary production (solid red) and PBH evaporation (solid blue) for $\mu_c = 10^{15}$ g, $\sigma = 1$, and $\rho_{\rm PBH} = 5.2 \times 10^{-11}$ GeV cm^{-3} (95 % CL UL from antiproton data). The total flux (solid black) assumes $\langle \phi_{FF} \rangle = 731$ MV; dashed and dot-dashed lines correspond to $\langle \phi_{FF} \rangle = 500$ MV and 900 MV, respectively. Shaded bands denote GAPS (blue) and AMS-02 (gray) sensitivities [18, 19].

parameters, and a rigorous statistical treatment of recent AMS-02 antiproton data. Our main findings are:

- **Universal spectral shapes:** PBH-induced antinuclei fluxes exhibit universal energy spectral shapes independent of the extended mass distribution parameters. The TOA fluxes peak at ∼1-2 GeV for antiprotons and at a few hundred MeV/n for antideuterons.
- **Competitive local PBH density and DM fraction limits:** AMS-02 antiproton data set stringent upper limits on the local PBH density (and hence on the PBH fraction of dark matter), rivaling or surpassing constraints from other cosmic messengers [17]. Including future GAPS low-energy antiproton data could improve these limits by a factor of ∼ 2.
- **Antideuteron prospects:** Even assuming the maximal local PBH density allowed by antiproton data, the predicted antideuteron flux remains below the projected sensitivities of both GAPS and AMS-02. Therefore, any future detection of antideuterons by these experiments could at most be only partially attributed to PBHs.

References

[1] S. Hawking, *Gravitationally collapsed objects of very low mass*, *Mon. Not. Roy. Astron. Soc.* **152** (1971) 75.

[2] KAGRA, VIRGO, LIGO Scientific collaboration, *GWTC-3: Compact Binary Coalescences Observed by LIGO and Virgo during the Second Part of the Third Observing Run*, *Phys. Rev. X* **13** (2023) 041039 [2111.03606].

[3] B. Carr and F. Kuhnel, *Primordial Black Holes as Dark Matter: Recent Developments*, *Ann. Rev. Nucl. Part. Sci.* **70** (2020) 355 [2006.02838].

[4] S.W. Hawking, *Black hole explosions*, *Nature* **248** (1974) 30.

[5] AMS collaboration, *The Alpha Magnetic Spectrometer (AMS) on the international space station: Part II — Results from the first seven years*, *Phys. Rept.* **894** (2021) 1.

[6] *GAPS contributions to the 38th International Cosmic Ray Conference (Nagoya 2023)*, 10, 2023.

[7] A. Dolgov and J. Silk, *Baryon isocurvature fluctuations at small scales and baryonic dark matter*, *Phys. Rev. D* **47** (1993) 4244.

[8] C. Arina, M. Di Mauro, N. Fornengo, J. Heisig, A. Jueid and R.R. de Austri, *CosmiXs: cosmic messenger spectra for indirect dark matter searches*, *JCAP* **03** (2024) 035 [2312.01153].

[9] M. Di Mauro, N. Fornengo, A. Jueid, R.R. de Austri and F. Bellini, *Nailing down the theoretical uncertainties of* $\overline{\mathrm{D}}$ *spectrum produced from dark matter*, 2411.04815.

[10] A. Arbey and J. Auffinger, *BlackHawk: A public code for calculating the Hawking evaporation spectra of any black hole distribution*, *Eur. Phys. J. C* **79** (2019) 693 [1905.04268].

[11] F. Calore, M. Cirelli, L. Derome, Y. Genolini, D. Maurin, P. Salati et al., *AMS-02 antiprotons and dark matter: Trimmed hints and robust bounds*, *SciPost Phys.* **12** (2022) 163 [2202.03076].

[12] D. Maurin, *USINE: Semi-analytical models for Galactic cosmic-ray propagation*, *Computer Physics Communications* **247** (2020) 106942 [1807.02968].

[13] M. Boudaud, Y. Génolini, L. Derome, J. Lavalle, D. Maurin, P. Salati et al., *AMS-02 antiprotons' consistency with a secondary astrophysical origin*, *Phys. Rev. Res.* **2** (2020) 023022 [1906.07119].

[14] Y. Génolini, M. Boudaud, M. Cirelli, L. Derome, J. Lavalle, D. Maurin et al., *New minimal, median, and maximal propagation models for dark matter searches with Galactic cosmic rays*, *Phys. Rev. D* **104** (2021) 083005 [2103.04108].

[15] N. Weinrich, M. Boudaud, L. Derome, Y. Genolini, J. Lavalle, D. Maurin et al., *Galactic halo size in the light of recent AMS-02 data*, *Astron. Astrophys.* **639** (2020) A74 [2004.00441].

[16] GAPS collaboration, *Sensitivity of the GAPS experiment to low-energy cosmic-ray antiprotons*, *Astropart. Phys.* **145** (2023) 102791 [2206.12991].

[17] P. De la Torre Luque, J. Koechler and S. Balaji, *Refining Galactic primordial black hole evaporation constraints*, *Phys. Rev. D* **110** (2024) 123022 [2406.11949].

[18] T. Aramaki, C. Hailey, S. Boggs, P. von Doetinchem, H. Fuke, S. Mognet et al., *Antideuteron sensitivity for the GAPS experiment*, **74** (2016) 6.

[19] T. Aramaki, S. Boggs, S. Bufalino, L. Dal, P. von Doetinchem, F. Donato et al., *Review of the theoretical and experimental status of dark matter identification with cosmic-ray antideuterons*, *Physics Reports* **618** (2016) 1.